Deciphering the Metal Speciation in Low-Molecular-Weight Complexes by IMS-MS: Application to the Detection of Manganese Superoxide Dismutase Mimics in Cell Lysates

Martha Zoumpoulaki, Gabrielle Schanne, Nicolas Delsuc, Hugues Preud'Homme, Elodie Quévrain, Nicolas Eskenazi, Géraldine Gazzah, Régis Guillot,, Philippe Seksik, Joelle Vinh, et al.

Deciphering the Metal Speciation in Low-Molecular-Weight Complexes by IMS-MS: Application to the Detection of Manganese Superoxide Dismutase Mimics in Cell Lysates

*Martha Zoumpoulaki, Gabrielle Schanne, Nicolas Delsuc, Hugues Preud'homme, Elodie Quévrain, Nicolas Eskenazi, Géraldine Gazzah, Regis Guillot, Philippe Seksik, Joelle Vinh, Ryszard Lobinski, and Clotilde Policar**

Abstract: The detection and quantification of exogenous metal complexes are crucial to understanding their activity in intricate biological media. Mn^{II} complexes are difficult to detect and quantify because of low association constants, and high lability. The superoxide dismutase (SOD) mimic (or mimetic) labelled Mn1 is based on a 1,2-di-aminoethane functionalized with imidazole and phenolate and has good intrinsic anti-superoxide, antioxidant and anti-inflammatory activities in lipopolysaccharide (LPS)-activated intestinal epithelial HT29-MD2 cells, similar to that of its propylated analogue labelled Mn1P. Ion mobility spectrometry-mass spectrometry (IMS-MS) is a powerful technique for separating low molecular weight (LMW) metal complexes and can even separate complexes with the same ligand but bound to different divalent metal cations with similar ionic radii. We demonstrated the intracellular presence of the Mn1 and Mn1P complexes, at least partly intact, in lysates of cells incubated with the complexes and estimated the intracellular Mn1P concentration using a Co-$^{13}C_6$ analogue.

Introduction

The reliable detection and quantification of exogenous metal complexes, such as metallodrugs or metal-based probes in intricate biological media, is essential for a good understanding of their bioactivity and can be particularly challenging. Various imaging techniques[1] based on fluorescence,[2–4] vibrational spectroscopies, including Fourier transform infrared spectroscopy (μ-FTIR),[5–12] μ-Raman,[13,14] laser ablation inductively coupled plasma mass spectrometry LA-ICP-MS,[15,16] or X-ray fluorescence (XRF)[5,17–29] can be used for the intracellular detection and mapping of metal complexes. Furthermore, mass spectrometry-based techniques,[30] such as ICP-MS,[30–33] electrospray ionization tandem mass spectrometry (ESI-MS/MS),[34] liquid chromatography-mass spectrometry (LC-MS),[35,36] as well as electron paramagnetic resonance (EPR)[25,37] or atomic absorption spectrometry (AAS),[35,38–44] have been used for their detection and quantification in cells or organisms.

Manganese(II) complexes, developed as contrast agents for magnetic resonance imaging (MRI),[45–51] or as catalytic antioxidants mimicking the mitochondrial manganese superoxide dismutase (MnSOD),[52–59] constitute a unique challenge. Biological environments are rich in Lewis bases[60] and contain a variety of divalent metal ions that constitute an exchangeable pool.[61] Due to their d^5 metal ion with no ligand-field-stabilization energy (LFSE),[25,62,63] Mn^{II} complexes display association constants in the low range of the Irving and Williams series.[64,65] Their d^5 configuration contributes to a low kinetic barrier to ligand dissociation or association,[25,62,63] and renders Mn^{II} complexes highly labile, with fast exchange of coordinated ligands and metal ions,[66,67] except for some very specific ligands specifically designed to achieve impressive inertness.[46] The knowledge

[*] Dr. M. Zoumpoulaki, G. Schanne, Dr. N. Delsuc, E. Quévrain, G. Gazzah, Prof. C. Policar
Laboratoire des biomolécules (LBM), Département de chimie, École normale supérieure, PSL University, Sorbonne Université, CNRS
75005 Paris (France)
E-mail: clotilde.policar@ens.psl.eu

Dr. M. Zoumpoulaki, Dr. N. Eskenazi, Dr. J. Vinh
SMBP ESPCI Paris, PSL University, UMR 8249 CNRS, (France)

Dr. M. Zoumpoulaki, G. Schanne, Prof. P. Seksik
Centre de Recherche de Saint-Antoine, INSERM, UMRS 938, Sorbonne University, INSERM
75012 Paris (France)

Dr. H. Preud'homme, Prof. R. Lobinski
Universite de Pau, CNRS, E2S, IPREM-UMR5254, Hélioparc, 64053 Pau (France)

Dr. R. Guillot
ICMMO UMR CNRS 8182Université Paris-Saclay,
91405 Orsay (France)

Prof. P. Seksik
Gastroenterology Department, Saint-Antoine Hospital, Sorbonne Université, APHP Paris, (France)

Prof. R. Lobinski
Chair of Analytical Chemistry, Warsaw University of Technology, Noakowskiego 3, 00-664 Warsaw (Poland)

of the speciation of a Mn^{II} complex or Mn^{II} ion in a biological environment is thus crucial.

A metal-free analytical environment is needed to avoid adventitious metal ion exchanges coming from the analytical system. Considering the plethora of species in the LMW range in cells, coupling of MS with a separation system is required. A comprehensive evaluation of high-performance liquid chromatography-mass spectrometry (HPLC-MS) for a large-scale study of metal complexes was reported elsewhere.[68] It has been also applied very recently to a more inert Mn-based complex similar to Mn1.[69] More labile compounds present additional problems, especially when they interact with the stationary phase and the tubing of the system. These interactions can lead to metal exchange and the decomposition of the target metal complexes.

Ion mobility spectrometry, first developed by Cohen and Karasek in 1970,[70] to detect traces of organic molecules in the gas phase, involves the movement of ions against a gas flow under an applied electric field. The velocity of ions is proportional to their reduced mobility constant K [$cm^{-1}V^{-1}s^{-1}$], which is associated with their rotationally averaged collision cross-section (*CCS*) also noted Ω (in $Å^2$). In IMS coupled with mass spectrometry, ion detection is performed using MS.[71–73] IMS-MS is a powerful technique used for structural characterization of biomolecules to probe the folding of proteins upon ligand binding,[74] and to study the dynamic of those interactions,[75] to characterize supramolecular complexes showing differences in host shape due to guest interaction.[76–79] It can also be used to separate species of very similar mobility with a high resolving power (>100 as defined by $\Omega/\Delta\Omega$ measured at full width at half maximum).[75] For instance, IMS-MS was used to characterize metal speciation in peptides.[80] Its application to the coordination of LMW ligands is not highly developed, probably because the change in shape upon folding around a metal ion is small, and as far as we know, IMS-MS has never been applied to study metal speciation[81] in LMW complexes in cell lysates.

We are interested in bioinspired metal-based catalytic antioxidants,[82–84] namely manganese(II) complexes that mimic SODs, metalloenzymes that catalyze the dismutation of superoxide and constitute the first line of cellular antioxidant defense.[52,54] One of these SOD mimics, Mn1 (Figure 1a), involves an open-chain ligand built on a 1,2-diamino-ethane scaffold, with two imidazole and one phenolate as appended coordinating moieties. Mn1 has good intrinsic anti-superoxide activity, as measured by the k_{cat} outside of a cellular context,[25,54] in line with its redox potential, which is close to the optimal SOD potential $E_{1/2}$ (V/SCE) typically ranging from 0 to 0.2 V/SCE, with an optimal value at 0.12 V/SCE,[52,54,82,85] which is the midpoint between $E^{0'}_{1/2}$ ($O_{2aq}/O_2^{\cdot-}$) = −0.42 V/SCE and $E^{0'}_{1/2}$($O_2^{\cdot-}$/H_2O_2) = 0.66 V/SCE.[86] One of the cellular models we use to evaluate SOD mimics[5,22,25,87,88] consists of intestinal epithelial cells, HT29-MD2, under lipopolysaccharide activation.[89,90] Mn1 displayed a good antioxidant and anti-inflammatory activity in this model, while its zinc(II) redox-inactive analogue, referred to as Zn1, and $MnCl_2$ showed no effect.[5,22,25,87] The quantification methods previously used (EPR, ICP-MS, XRF)[5,22,25] were focused on the metal ion cellular content and its comparison with the endogenous content, assuming that excess of Mn was due to internalized Mn1. This could have some drawbacks as incubation with a non-native coordination complex may itself alter the homeostasis of the metal ions within the cells*. To avoid this possible bias and to also determine the amount of intact metal complex in cells, we wanted to directly track it in cell lysates. We showed previously using LC/MS-MS,[25] that Mn1 penetrates the cells but the fact that the m/z peak of $[Mn1]^+$ (408.1465) is very close to that of the m/z peak of $[Fe1-H]^+$ (408.1355), with overlapping isotopic patterns prevented any reliable quantitative analysis, as previously performed with a more inert analogue.[69] Recently, to investigate the Mn1 subcellular location, a multimodal Re-tris carbonyl probe was conjugated to the ligand. The Mn^{II} complex showed the same activity as Mn1 but a different cellular distribution. Tagging the ligand was used as an indirect way to study speciation. Mn and Re were only partially colocalized, suggesting possible dissociation.[5]

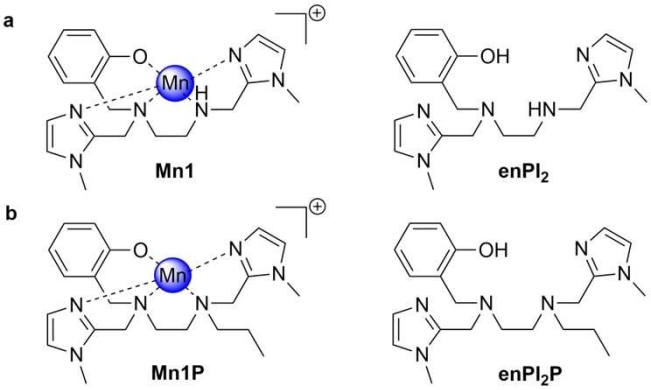

Figure 1. Chemical structure of MnSOD mimics. a) Mn1 and $enPI_2$ ligand. b) Propylated analogue Mn1P and $enPI_2P$ ligand. The analogues with Zn^{II}, not shown in this figure, were labeled Zn1 and Zn1P similar to other metal cations (Co1, Fe1, Cu1, etc.).

This study aims to elucidate the fate of Mn1 and its propylated analogue Mn1P (Figure 1b) in HT29-MD2 cell lysates using MS-based methods. To match the conditions under which we study the anti-inflammatory and antioxidant activity of the SOD mimics[5,22,25] (Figure 2), we co-incubated the SOD mimics with LPS. The fact that Mn of natural abundance is monoisotopic precludes considering mass isotopic distribution to ascertain whether a Mn complex is present. We have explored here IMS-MS to demonstrate unambiguously the intracellular presence of the intact Mn1 and Mn1P complexes (Mn^{II}-Ligand) and to estimate the intracellular concentration of Mn1P.

Results and Discussion

Physico-Chemical Properties of Mn1 and Mn1P

Anticipating possible issues with deprotonation of the NH group in Mn1 during MS experiments, we decided to

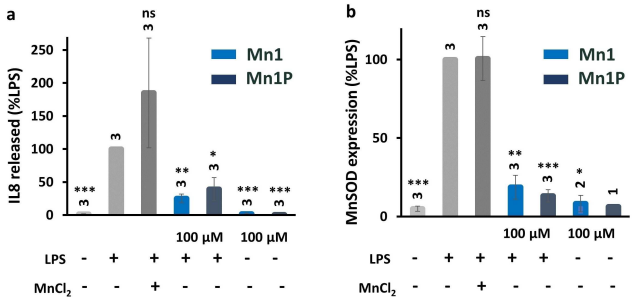

Figure 2. Anti-inflammatory and antioxidant activity of Mn1 and Mn1P. LPS-activated (0.1 µg mL^{-1}) cells were incubated in the presence of $MnCl_2$, Mn1, or Mn1P at 100 µM for 6 h. Non-activated cells were incubated with cell media, Mn1 or Mn1P at 100 µM for 6 h. Positive and negative controls consist of LPS-activated and non-activated HT29-MD2 cells (light grey), respectively. a) Quantification of interleukin 8 (IL-8) inflammation chemokine, in supernatants, measured by ELISA. The IL-8 amount was normalized by the total protein amount in each sample and was reported as ng/mg of proteins. Normalized IL-8 amount is presented % vs. the LPS positive control. Results represent mean ± SEM for three biological experiments in technical duplicates. b) MnSOD expression in cell lysates measured by Western Blot. MnSOD expression was normalized to the total amount of protein in each sample. Normalized MnSOD expression intensity is presented % vs. the LPS positive control. Data represent mean ± SEM with the number of independent experiments indicated above each column. The p-values were calculated using the Student's t-test. The mean rank of each column was compared to that of the LPS control, each comparison stands alone. (***) $p < 0.001$, (**) $p < 0.01$, and (*) $p < 0.05$ versus LPS control, and ns means nonsignificant.

derivatize the secondary amine of the 1,2-diamino-ethane scaffold by adding a propyl chain leading to Mn1P. Mn1P was prepared as Mn1[5,22,25] using a propylated version of the $enPI_2$ ligand as described elsewhere.[69] The functionalization of the nitrogen with a propyl group did not greatly alter the properties of the SOD mimic, as shown in Tables 1 and 2, and Figures 2, S1a–d. Mn1P showed a peak higher than Mn1 when analyzed in 1/1 ratio by ESI-MS, indicating better ionization properties for Mn1P (Figure S1e). The crystallographic structure of Mn1P consists of the dimeric $[(enPI_2P)Mn\,Mn\,(enPI_2P)](PF_6)_2$, with each Mn^{II} ion hexacoordinate with four nitrogen atoms of the anionic form $enPI_2P^-$ of the ligand and two bridging oxygen atoms from the phenolate groups (Tables S1 and S2, Figure S2). As for Zn1,[5,22,25] the redox inactive analogue Zn1P did not demonstrate any anti-inflammatory activity in inflamed HT29-MD2 cells (Figure S3). None of the above-mentioned complexes was cytotoxic (Figure S4).

Table 1: Comparison of Mn1P and Mn1 physicochemical properties (HEPES, 50 mM, pH 7.5).

	Mn1	Mn1P
Redox potential $E_{1/2}$ [V/SCE][a]	0.20	0.21
SOD activity[b]	$IC_{50} = 1.26$ µM $\text{Log}\,k_{cat} = 7.31$	$IC_{50} = 1.26$ µM $\text{Log}\,k_{cat} = 7.32$

[a] Measured with a 200 µM solution of the complexes in HEPES (50 mM, pH 7.5), with a Pt auxiliary electrode and a glassy carbon disk as working electrode, at scan rates 0.1 or 0.2 V s. See Supporting Information for additional details. [b] Measured using the Fridovich assay,[54,83,91,92] in HEPES (50 mM, pH 7.5), with cytochrome *c* Fe^{III} as UV/Visible marker, [CytcFe(III)] = 100 µM. See Supporting Information for additional details.

IMS-MS: A Powerful Analytical Technique to Discriminate between LMW Complexes with Similar Divalent Metal Ions

We investigated whether IMS-MS could discriminate between the same LMW ligand bound to various divalent metal cations from the first series of the transition elements or Zn^{II}, that are folded differently due to small changes in ionic radii.[93] The capacity to distinguish two species with a close *CCS*, is dependent on the capacity to separate two peaks. If we consider that two peaks of equal intensity are resolved if the valley between them is less than 0.1 of the peak intensity, the minimum difference in mobility allowing the distinction among two species is close to 2 Å^2 *CCS* difference. Table 3 gives the *CCS* and inverse of the reduced mobility constant K_0[73] for a series of complexes derived from $enPI_2$ and $enPI_2P$, namely Mn1 and its analogues Zn1, Ni1, Fe1, Co1, Cu1 on the one hand, and Mn1P and its analogues Zn1P, Ni1P, Fe1P, Co1P, Cu1P, on the other hand (see also Figure 3). Mobilograms extracted at a given molecular mass for each of these complexes analyzed separately are presented in Figure 4, as an overlay. Figure S6 shows that the various complexes can be identified in an equimolar mixture of complexes. These data show that the discrimination between the complexes is achievable in both series, with *CCS* ranging from 180.557 to 188.124 Å^2 for $enPI_2$ and from 190.825 to 197.485 Å^2 for $enPI_2P$.

The observed ion mobilities of the metallated forms correlate well with theoretical ionic radii of the divalent transition metal cations (high spin, pentacoordinate) [$Mn^{II} > Fe^{II} > Co^{II} > Zn^{II} > Ni^{II} > Cu^{II}$], except Fe1P whose MS peak shows the presence of an additional water molecule (Figure 3, Table 3).[93] Metal complexes can form hydrogen bonds with water molecules when in solution.[94] The differ-

Table 2: Association constants K_{ML} (equivalent to M^{-1}) of the studied ligands with Mn^{II}, Co^{II}, and Zn^{II}.[a]

Ligand	K_{MnL}	K_{CoL}	K_{ZnL}
$L = enPI_2$	$1.22 \pm 0.18 \times 10^6$	$1.10 \pm 0.62 \times 10^8$	$1.0 \pm 0.2 \times 10^{10}$
$L = enPI_2P$	$1.04 \pm 0.18 \times 10^6$	$2.30 \pm 1.32 \times 10^7$	$6.0 \pm 1.4 \times 10^9$

[a] Measurements were performed in a HEPES 50 mM buffer at pH 7.5 with an ionic strength of 12.5 mM and at 25 °C (see Figure S5 for Co^{II} and Supporting Information for experimental details). Association constants of the complexes with Cu^{II} and Fe^{II}, less relevant in this study, are given only in the Supporting Information for information.

Table 3: IMS-MS data of the metallated forms of the $enPI_2$ and $enPI_2P$ ligand (with Mn^{II}, Fe^{II}, Co^{II}, Ni^{II}, Cu^{II}, Zn^{II}, as in the order of the periodic table).[a]

Name	Species	*m/z* $[L+M]^+$ exp	*m/z* $[L+M]^+$ calc	δm [ppm]	$1/K_0$ [$cm^2V^{-1}s^{-1}$]	CCS [$Å^2$]	r_{ion} [Å]
$enPI_2$	$[enPI_2+H]^+$	355.22404	355.2241	0.14	0.8607 ± 0.001	181.109	–
Mn1	$[enPI_2+Mn]^+$	408.14615	408.1465	0.80	0.8983 ± 0.001	188.124	0.75
Mn1-H	$[enPI_2+Mn-H]^+$	407.13839	407.13865	0.65	0.8621 ± 0.001	180.557	–
Fe1-H	$[enPI_2+Fe-H]^+$	408.13570	408.1355	−0.33	0.8926 ± 0.001	186.932	0.78
Co1	$[enPI_2+Co]^+$	412.14131	412.1416	0.77	0.8922 ± 0.001	186.788	0.67
Ni1	$[enPI_2+Ni]^+$	414.14356	411.1438	0.52	0.8895 ± 0.001	186.226	0.63
Cu1	$[enPI_2+Cu]^+$	416.13796	416.1380	0.18	0.8837 ± 0.001	184.944	0.65
Zn1	$[enPI_2+Zn]^+$	417.13732	417.1376	0.62	0.8922 ± 0.001	186.697	0.68
$enPI_2P$	$[enPI_2P+H]^+$	397.27043	397.2710	1.53	0.9104 ± 0.001	190.825	–
Mn1P	$[enPI_2P+Mn]^+$	450.19296	450.1934	1.05	0.9344 ± 0.001	195.096	0.75
Fe1P	$[enPI_2P+H_2O+Fe]^+$	468.19296	468.19306	0.27	0.9469 ± 0.001	197.485	0.78
Co1P	$[enPI_2P+Co]^+$	454.18858	454.1886	0.24	0.9299 ± 0.001	194.107	0.67
Ni1P	$[enPI_2P+Ni]^+$	453.19023	453.1907	1.09	0.9254 ± 0.001	193.170	0.63
Cu1P	$[enPI_2P+Cu]^+$	458.18474	458.1850	0.53	0.9218 ± 0.001	192.360	0.65
Zn1P	$[enPI_2P+Zn]^+$	459.18433	459.1845	0.44	0.9290 ± 0.001	193.840	0.68

[a] MS and IMS parameters determined after injection at neutral pH (20 μM in 20% NH_4HCO_3 50 mM pH 7.4/80% acetonitrile or ACN). *m/z [L+M]+ exp* refers to the experimental *m/z* value of each species, whereas *m/z [L+M]+calc* refers to the corresponding theoretical calculated *m/z* value. *δm* describes the precision of the measure (*m/z*) (in ppm, or $[(m/z)_{measured}-(m/z)_{theoretical}]/(m/z)_{theoretical}\times10^6$). K_0 is the reduced mobility constant, with $K_0 = K\times(273/T)\times(P/760)$, where *K* is the mobility coefficient of the ion in $cm^2V^{-1}s^{-1}$, *T* is the absolute temperature in Kelvin (fixed at 298 K) and *P* is the pressure in Torr of the N_2 gas through which ions move (set to get an accurate CCS for a *m/z* 622 compound). The *CCS* (or Ω) is related to the ion mobility according to the following equation: $K = 3/16_*\sqrt{(2\pi/\mu\times k_B\times T)}\times(ze/N\times\Omega)$, where μ is the reduced mass of the ion-gas pair ($\mu = mM/(m+M)$, with m and M the ion and gas-particle masses), k_B is the Boltzmann constant, and *ze* is the analyte charge.[95] r_{ion} is the ionic radius of metal cations in Å. Note that he *CCS* values measured here are highly reproducible with replicates having <0.3% relative standard deviation (RSD) (<0,6% in previous work for traveling wave mobility techniques).[96,97] Typically, the RSD values reported in the literature are <2% deviation (uniform field mobility techniques)[98] (see Supporting Information for further details).

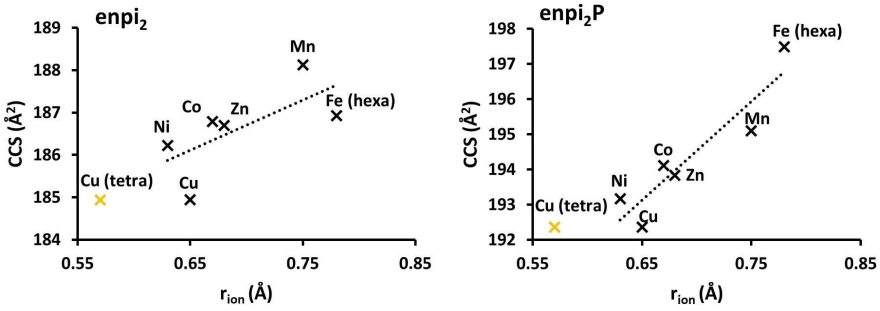

Figure 3. Collision cross-section in $Å^2$ plotted against the ionic radius of metal cations in Å. The r_{ion} of any M^{II} corresponds to a high spin penta-coordination, except for Fe^{II} (high-spin hexa-coordination). The r_{ion} for Cu^{II} is also shown (in yellow) for a high-spin tetra-coordination. The r_{ion} values were taken from http://abulafia.mt.ic.ac.uk/shannon/ptable.php.[76]

ence between Fe1 and Fe1P may be related to the presence of a more hydrophobic environment for Fe1P (presence of an additional propyl group) which protects Fe1P from the loss of a water molecule. In the case of $enPI_2$ and Cu^{II}, the correlation with *CCS* matched better with an ionic radius for a high spin tetra-coordination, maybe suggesting a partial ligand dechelation (Figure 3). Overall, this specificity of *CCS* with the coordinated metal ions opens up interesting perspectives for the study of speciation in LMW metal complexes and, here, for the characterization of the complexes in cell lysates after cell incubation with Mn1 or Mn1P. Note that the intensity of peaks in the mobilograms does not depend on the ion mobility but on the efficiency of electrospray ionization of a metal complex. No models allowing a correlation of the efficiency of electrospray ionization with the structure of metal complexes are available.

Towards the Use of IMS-MS to Detect SOD Mimics in Cell Lysates

ESI-MS with a metal-free ionization source allowed the detection of Mn1 (resp. Mn1P) at *m/z* 408.1465 (resp. *m/z* 450.1935) (Figure S7a) by direct infusion of pure Mn1 (resp. Mn1P) solutions (50 μM in 20% NH_4HCO_3 50 mM pH 7.4/80% ACN). Optimal ionization was observed for 80% ACN (Figure S8). No other metal ions were observed in the pure Mn1 (resp. Mn1P) samples when analyzed by ICP-MS (Figure S9). When cell-lysates of LPS-activated HT29-MD2

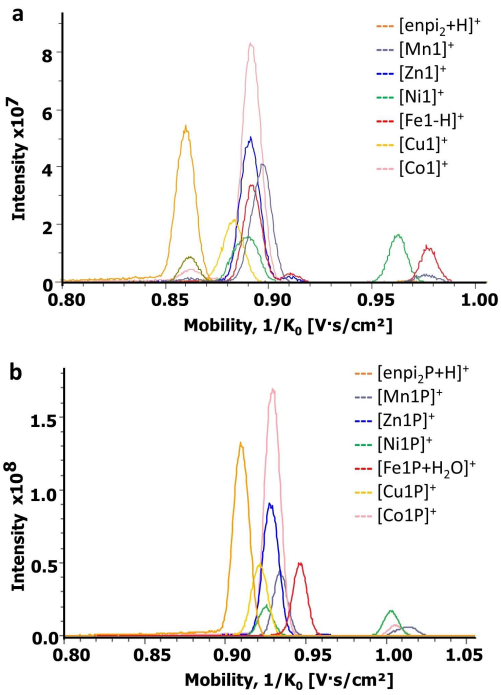

Figure 4. Overlay of extracted ion mobilograms of pure solutions of each complex (20 μM). a) IM of $[enPI_2+H]^+$, $[Mn1]^+$, $[Zn1]^+$, $[Ni1]^+$, $[Fe1-H]^+$, $[Cu1]^+$, $[Co1]^+$ and b) $[enPI_2P+H]^+$, $[Mn1P]^+$, $[Zn1P]^+$, $[Ni1P]^+$, $[Fe1P+H_2O]^+$, $[Cu1P]^+$, $[Co1P]^+$ were extracted with their corresponding theoretical *m/z* (see Table S3) with 5 mDa precision. All complexes were analyzed separately at 20 μM in 80% ACN/20% NH_4HCO_3 50 mM pH 7.4.

cells incubated with Mn1 (100 μM, 6 h) were analyzed using direct infusion in ESI-MS, the peak of Mn1 was not seen amongst other more abundant cellular species (Figure S7b), highlighting the need for a second dimension. Note that using LC-ESI-MS, when we analyzed pure Mn1 in solution, complexes with divalent transition metals other than Mn^{II} were observed, showing the release of transition metals ions from the analytical system (Figure S10).

Interestingly, no metal exchange was detectable from a pure solution Mn1 (resp. Mn1P) at 50 μM when analyzed by IMS-MS direct infusion (Figures S11a, 12a). Similarly, when the ligands, $enPI_2$ and $enPI_2P$, were injected, they were not found metallated (Figures S11b, 12b), highlighting the fact that at 50 μM, no contamination from the analytical system was detectable. Nevertheless, when pure solutions of Mn1 or Mn1P were injected at lower concentrations, some exchange with Zn was observed. When Mn1 was injected at 2 μM, although the Mn analogue was the more abundant species, a peak ratio of $[Zn1]^+/[Mn1]^+$ of 1/3 was observed, and $[Zn1]^+$ contribution was higher than $[Mn1]^+$ when a solution of Mn1 at 0.02 μM was injected (Figure S13a). Similarly, the $[Zn1P]^+/[Mn1P]^+$ ratio was 1/8 when Mn1P was injected at 2 μM and was 1/3 when injected at 0.02 μM (Figure S14a). Clearly, when comparing Figure S13a and S14a, one can tell that Mn1P experienced less exchange with Zn than Mn1, especially at lower concentrations.

We then explored the effect of the cellular medium. When Mn1 or Mn1P were added to cell lysates at 2 μM, the Zn analogues were the more abundant species both with Mn1 and Mn1P. This showed that the Zn^{II} contribution from the cell lysates exceeded the zinc contribution from the IMS-MS system (Figure S13b, S14b), which can then be disregarded. Thus, 2 μM is the threshold for the detection of these Mn-complexes in cell lysates, with minimal interferences from the analytical IMS-MS system.

Application of IMS-MS to Detect and Quantified SOD Mimics in Cell Lysates Using a Heavy-Ligand ($^{13}C_6$) Co-analogue

Direct infusion IMS-MS was used for Mn complexes detection in HT29-MD2 cell lysates after cell incubation with LPS at 0.1 $\mu g\,mL^{-1}$ and the compounds at 100 μM for 6 h (see Supporting Information, Figure S15). The complexes were detected in cell lysates in extracted exact mass and exact ion mobilogram of Mn1 or Mn1P (Figure 5a, b, d, e). Thus, combining two orthogonal dimensions (ion mobility and exact mass) is an efficient approach for characterizing metal complexes in intricate biological environments, showing here unambiguously that both Mn1 and Mn1P are present intact in lysates of cells incubated with the compounds.

In addition to the IMS-MS signature of Mn1 (resp. Mn1P), we extracted peaks corresponding to Zn1 (resp. Zn1P), indicating metal exchanges (Figures 5c–f, S16). In the case of Mn1, we also observed peaks resulting from dehydrogenation (Mn1-H and Fe1-H overlapping with Mn1) (Figure 5c). Interestingly, IMS-MS is powerful enough to distinguish between isobaric Mn1 and Fe1-H. However, the overlapping of the peaks prevented a reliable quantification of low cellular levels of Mn1. Since Mn1P undergoes fewer metal exchange events in cells (Figure S16) and cannot be dehydrogenated (Figure 5f), it was the most suitable candidate to attempt intracellular quantification using an internal standard.

We decided to use $Co1^{13}C_6P$ (Figure 6a) as an internal standard because a) $Co1^{13}C_6P$ and Mn1P are structurally very similar and possess the same charge, b) Co^{II} is not naturally present in cells, c) no metal exchange was observed for $Co1^{13}C_6P$ (resp. $enPI_2{}^{13}C_6P$) at 50 μM by IMS-MS (Figure S17) and d) no exchange was observed between Mn1P and $Co1^{13}C_6P$, or between Zn1P and $Co1^{13}C_6P$ (1:1 by ESI-MS) even after 24 h (Figure S18). This showed that $Co1^{13}C_6P$ was sufficiently stable and inert. Using a heavy analogue of the ligand ($enPI_2{}^{13}C_6P$ instead of $enPI_2P$) has the additional advantage to enable tracking of possible exchange between Mn1P and the standard in cell lysates, and little exchange of Co–Zn was seen in cell lysates. As the intensities are dependent on the ionization properties of Mn1P and Co1P (see Figure 4b), a calibration curve was established in a pure buffer/ionization solution for the quantification of Mn1P (Figure S19). After incubation with Mn1P and LPS, the cell lysates (see Supporting Information) were spiked with $Co1^{13}C_6P$ at 0.02 μM. The estimate of Mn1P concentration in the injected solution of cell lysate

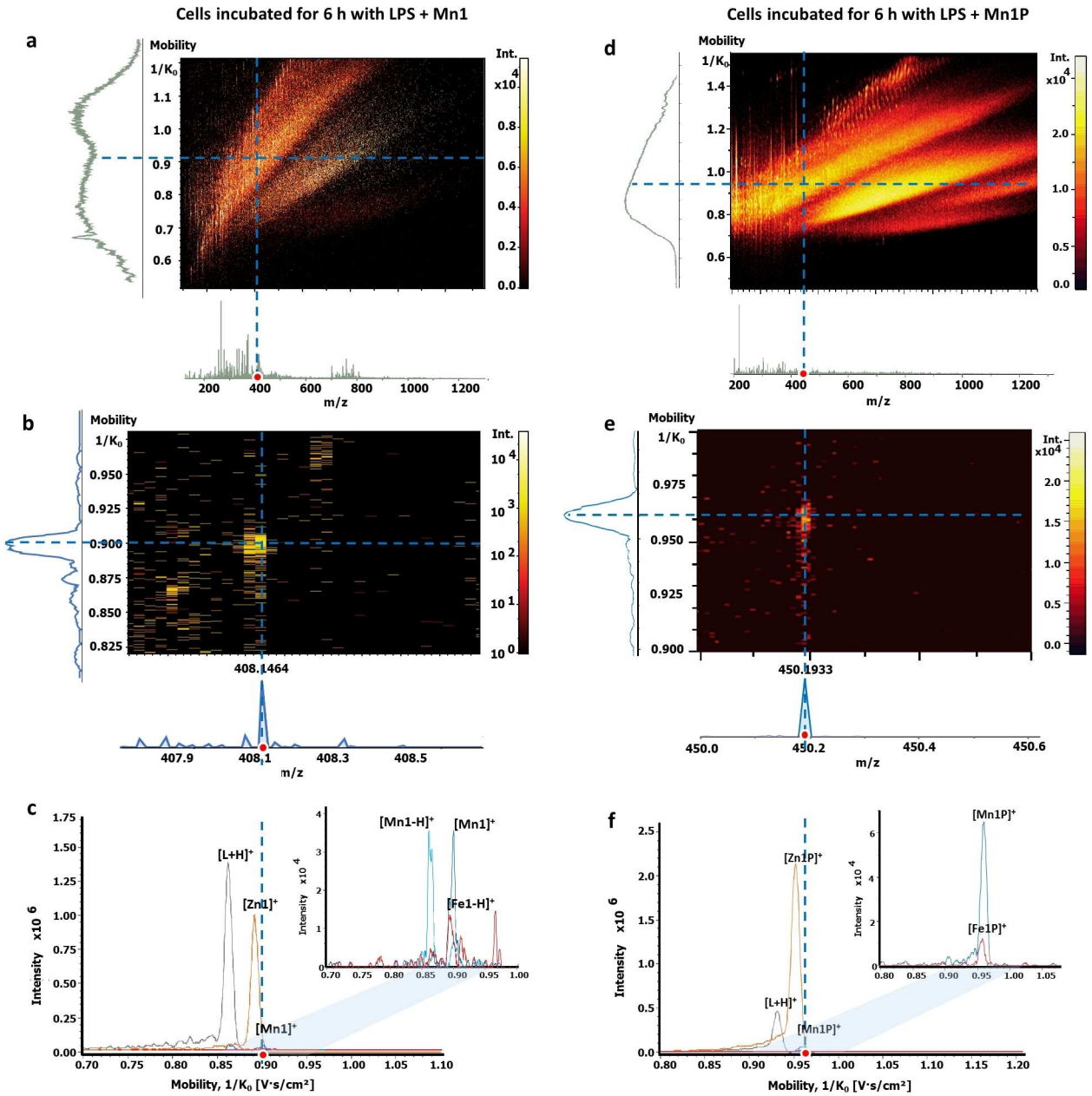

Figure 5. Detection of Mn1 and Mn1P in cell lysates by IMS-MS. Cells were incubated with Mn1 or Mn1P (100 μM) and LPS (0.1 μg mL^{-1}) for 6 h and corresponding cell lysates were ionized in 80% ACN/20% NH_4HCO_3 50 mM pH 7.4. Full heat map with corresponding IMS and MS spectra for a) Mn1 and d) Mn1P. Extracted heat map with corresponding IMS and MS spectra for b) Mn1 and e) Mn1P. The IM of $[Mn1]^+$ was extracted at 408.1465 *m/z*, 0.909 V s cm^{-2}, and of $[Mn1P]^+$ at 450.1933 *m/z*, 0.960 V s cm^{-2} with 5 mDa precision. Corresponding extracted ion mobilograms for c) Mn1 and f) Mn1P. The IM of $[Mn1]^+$, $[Mn1-H]^+$, $[Fe1-H]^+$, $[L+H]^+$, $[Zn1]^+$ and $[Mn1P]^+$, $[Fe1P]^+$, $[LP+H]^+$, $[Zn1P]^+$ were extracted with their corresponding theoretical *m/z* (see Table S3) with 5 mDa precision.

(see Supporting Information) was 0.017 ± 0.005 μM (corresponding to 0.093 ± 0.028 μM in the cell lysate). The intracellular Mn1P concentration was estimated at 0.013 ± 0.006 fmol/cell (Figures 6b, S19, Table S4). This value corresponds to a minimal quantity of Mn1P found in the cells, as exchange or dissociation may have occurred during the lysis process and sample preparation, associated with the possible release of metal cation, here seemingly mainly Zn^{II}, from biological coordination and dilution.

Conclusion

In summary, we have demonstrated that the intracellular detection of the Mn1 and Mn1P SOD mimics can be performed using IMS-MS. This technique allowed efficient discrimination between the various metallic analogues of LMW complexes. This study exemplifies the IMS-MS potential for LMW molecules with the same charge and minor shape changes associated with small ionic radius differences between metal ions: for instance, Fe1 and Mn1

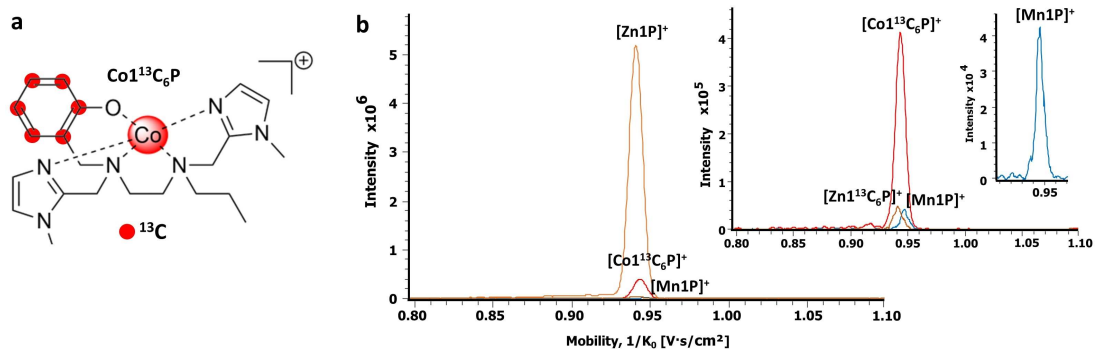

Figure 6. Quantification of Mn1P in cell lysates. a) Chemical structure of $^{13}C_6$-labeled propylated internal standard (Co1^{13}C$_6$P). b) Extracted ion mobilogram of cell lysate from cells incubated with Mn1P (100 μM) and LPS (0.1 μg mL^{-1}) for 6 h, spiked with Co1^{13}C$_6$P at 0.02 μM, just before IMS-MS analysis in 80% ACN/20% NH_4HCO_3 50 mM pH 7.4. The IM of [Co1^{13}C$_6$P]$^+$, [Mn1P]$^+$, [Zn1P]$^+$, [Zn1^{13}C$_6$P]$^+$ were extracted with their corresponding theoretical *m/z* (see Table S3) with 5 mDa precision.

with $\Delta r_{ion}/r_{ion}$ of 4% could be distinguished by IMS-MS. Compared to LC-MS, very little metal released was observed from the IMS-MS analytical system, which allowed the characterization of labile complexes with negligible metal exchange from the analytical system. Therefore, the two-dimensionality of IMS-MS, involving both ion mobility and *m/z* ratio can be used to track LMW complexes in an intricate environment such as cell lysate. This study shows unambiguously that both intact Mn1 and Mn1P are present in cell lysates after cells incubation with the complexes. In the case of Mn1P, we were able to establish a dynamic range to analyze the cell lysates for which the metal exchange was associated, not with the analytical system, but only with the metal ions pool from the cell lysate. Quantification with a heavy $^{13}C_6$-Co analogue allowed us to estimate the content of Mn1P in cells.

Acknowledgements

ANR (ANR-10-IDEX-0001-02 PSL* and ANR-15-CE07-0027-MAGIC), Fondation pour la Recherche Biomédicale (DEI20151234413), IDEX ENS-PSL (ANR-10-IDEX-0001-02 PSL*) are acknowledged for financial support and M.Z.'s Ph.D. fellowship (ANR-15-CE07-0027-MAGIC). Sorbonne Université and the program IPV (interface pour le vivant) are acknowledged for G.S.'s Ph.D. fellowship, Conseil scientifique régional Ile de France for financial support (Sesame 2010-10022268 & 2018-EX039194). Financial support from the National FT-ICR network (FR 3624 CNRS) is gratefully acknowledged. CNRS and the program MITI (mission pour les initiatives transverses et l'interdisciplinarité) are acknowledged for funding (call Metallomix, project ANACOMDA). We thank ENS-PSL, Sorbonne Université, CNRS for recurrent funding. We thank S. Shakir for help with LC-MS, B. Goetz and P. Legeay for help with ICP-MS, and L. Brot for help with cell culture.

Conflict of Interest

P. Seksik has received personal fees from Takeda, Merck MSD, Biocodex, Ferring, Fresenius Kabi, Astellas, Amgen, Pfizer, Pilege and Abbvie but has no conflict of interest linked to this work.

Data Availability Statement

The data that support the findings of this study are available in the Supporting Information of this article.

*We thank one of the reviewers for this wise remark, that gives the efforts for detecting whole SOD mimics in cell lysates additional value.

Keywords: Bioinorganic Chemistry · Intracellular Detection · Ion Mobility Spectroscopy · Manganese(II) Superoxide Dismutase Mimics or Mimetics · Mass Spectrometry

[1] R. McRae, P. Bagchi, S. Sumalekshmy, C. J. Fahrni, *Chem. Rev.* **2009**, *109*, 4780–4827.
[2] S. Banerjee, A. R. Chakravarty, *Acc. Chem. Res.* **2015**, *48*, 2075–2083.
[3] T. Zou, C. T. Lum, S. S.-Y. Chui, C.-M. Che, *Angew. Chem. Int. Ed.* **2013**, *52*, 2930–2933; *Angew. Chem.* **2013**, *125*, 3002–3005.
[4] F. Schmitt, P. Govindaswamy, G. Süss-Fink, W. H. Ang, P. J. Dyson, L. Juillerat-Jeanneret, B. Therrien, *J. Med. Chem.* **2008**, *51*, 1811–1816.
[5] E. Mathieu, A.-S. Bernard, E. Quévrain, M. Zoumpoulaki, S. Iriart, C. Lung-Soong, B. Lai, K. Medjoubi, L. Henry, S. Nagarajan, F. Poyer, A. Scheitler, I. Ivanović-Burmazović, S. Marco, A. Somogyi, P. Seksik, N. Delsuc, C. Policar, *Chem. Commun.* **2020**, *56*, 7885–7888.
[6] F. Zobi, L. Quaroni, G. Santoro, T. Zlateva, O. Blacque, B. Sarafimov, M. C. Schaub, A. Yu Bogdanova, *J. Med. Chem.* **2013**, *56*, 6719–6731.
[7] K. V. Kong, W. Chew, L. H. K. Lim, W. Y. Fan, W. K. Leong, *Bioconjugate Chem.* **2007**, *18*, 1370–1374.

[8] S. Clède, N. Cowan, F. Lambert, H. C. Bertrand, R. Rubbiani, M. Patra, J. Hess, C. Sandt, N. Trcera, G. Gasser, J. Keiser, C. Policar, *ChemBioChem* **2016**, *17*, 1004–1007.

[9] L. Henry, N. Delsuc, C. Laugel, F. Lambert, C. Sandt, S. Hostachy, A.-S. Bernard, H. C. Bertrand, L. Grimaud, A. Baillet-Guffroy, C. Policar, *Bioconjugate Chem.* **2018**, *29*, 987–991.

[10] S. Clède, N. Delsuc, C. Laugel, F. Lambert, C. Sandt, A. Baillet-Guffroy, C. Policar, *Chem. Commun.* **2015**, *51*, 2687–2689.

[11] S. Clède, F. Lambert, C. Sandt, Z. Gueroui, M. Réfrégiers, M.-A. Plamont, P. Dumas, A. Vessières, C. Policar, *Chem. Commun.* **2012**, *48*, 7729.

[12] C. Policar, J. B. Waern, M.-A. Plamont, S. Clède, C. Mayet, R. Prazeres, J.-M. Ortega, A. Vessières, A. Dazzi, *Angew. Chem. Int. Ed.* **2011**, *50*, 860–864; *Angew. Chem.* **2011**, *123*, 890–894.

[13] P. Hildebrandt, *Angew. Chem. Int. Ed.* **2010**, *49*, 4540–4541; *Angew. Chem.* **2010**, *122*, 4642–4644.

[14] K. Meister, J. Niesel, U. Schatzschneider, N. Metzler-Nolte, D. A. Schmidt, M. Havenith, *Angew. Chem. Int. Ed.* **2010**, *49*, 3310–3312; *Angew. Chem.* **2010**, *122*, 3382–3384.

[15] J. S. Becker, *J. Mass Spectrom.* **2013**, *48*, 255–268.

[16] L. Mueller, A. J. Herrmann, S. Techritz, U. Panne, N. Jakubowski, *Anal. Bioanal. Chem.* **2017**, *409*, 3667–3676.

[17] J. H. Lovett, H. H. Harris, *Curr. Opin. Chem. Biol.* **2021**, *61*, 135–142.

[18] E. M. Bolitho, C. Sanchez-Cano, H. Shi, P. D. Quinn, M. Harkiolaki, C. Imberti, P. J. Sadler, *J. Am. Chem. Soc.* **2021**, *143*, 20224–20240.

[19] F. Fus, Y. Yang, H. Z. S. Lee, S. Top, M. Carriere, A. Bouron, A. Pacureanu, J. C. da Silva, M. Salmain, A. Vessières, P. Cloetens, G. Jaouen, S. Bohic, *Angew. Chem. Int. Ed.* **2019**, *58*, 3461–3465; *Angew. Chem.* **2019**, *131*, 3499–3503.

[20] A. Enriquez Garcia, B. Lai, S. G. Gopinathan, H. H. Harris, C. S. Shemanko, F. Jalilehvand, *Chem. Commun.* **2019**, *55*, 8223–8226.

[21] J. J. Conesa, A. C. Carrasco, V. Rodríguez-Fanjul, Y. Yang, J. L. Carrascosa, P. Cloetens, E. Pereiro, A. M. Pizarro, *Angew. Chem. Int. Ed.* **2020**, *59*, 1270–1278; *Angew. Chem.* **2020**, *132*, 1286–1294.

[22] E. Mathieu, A.-S. Bernard, H. Y. V. Ching, A. Somogyi, K. Medjoubi, J. R. Fores, H. C. Bertrand, A. Vincent, S. Trépout, J.-L. Guerquin-Kern, A. Scheitler, I. Ivanović-Burmazović, P. Seksik, N. Delsuc, C. Policar, *Dalton Trans.* **2020**, *49*, 2323–2330.

[23] S. Hostachy, M. Masuda, T. Miki, I. Hamachi, S. Sagan, O. Lequin, K. Medjoubi, A. Somogyi, N. Delsuc, C. Policar, *Chem. Sci.* **2018**, *9*, 4483–4487.

[24] S. Hostachy, C. Policar, N. Delsuc, *Coord. Chem. Rev.* **2017**, *351*, 172–188.

[25] E. Mathieu, A.-S. Bernard, N. Delsuc, E. Quévrain, G. Gazzah, B. Lai, F. Chain, P. Langella, M. Bachelet, J. Masliah, P. Seksik, C. Policar, *Inorg. Chem.* **2017**, *56*, 2545–2555.

[26] C. M. Weekley, I. Kenkel, R. Lippert, S. Wei, D. Lieb, T. Cranwell, J. L. Wedding, A. S. Zillmann, R. Rohr, M. R. Filipovic, I. Ivanović-Burmazović, H. H. Harris, *Inorg. Chem.* **2017**, *56*, 6076–6093.

[27] S. Clède, C. Policar, *Chem. Eur. J.* **2015**, *21*, 942–958.

[28] J. B. Aitken, E. L. Shearer, N. M. Giles, B. Lai, S. Vogt, J. S. Reboucas, I. Batinic-Haberle, P. A. Lay, G. I. Giles, *Inorg. Chem.* **2013**, *52*, 4121–4123.

[29] J. B. Waern, H. H. Harris, B. Lai, Z. Cai, M. M. Harding, C. T. Dillon, *J. Biol. Inorg. Chem.* **2005**, *10*, 443–452.

[30] C. Ionescu, P. Grill, H. Witte, C. Boigues, A. Blanchard, B. Löffler, B. Michalke, *J. Trace Elem. Med. Biol.* **2019**, *56*, 207–212.

[31] M. R. M. Williams, B. Bertrand, D. L. Hughes, Z. A. E. Waller, C. Schmidt, I. Ott, M. O'Connell, M. Searcey, M. Bochmann, *Metallomics* **2018**, *10*, 1655–1666.

[32] S. P. McCormick, M. J. Moore, P. A. Lindahl, *Biochemistry* **2015**, *54*, 3442–3453.

[33] M. Groessl, O. Zava, P. J. Dyson, *Metallomics* **2011**, *3*, 591–599.

[34] M. Tsednee, Y.-C. Huang, Y.-R. Chen, K.-C. Yeh, *Sci. Rep.* **2016**, *6*, 1–13.

[35] J. Wojcieszek, P. Kwiatkowski, L. Ruzik, *J. Chromatogr. A* **2017**, *1492*, 70–78.

[36] C. Støving Dam, S. Alejo Perez Henarejos, T. Tsolakou, C. Alexander Segato, B. Gammelgaard, G. S. Yellol, J. Ruiz, I. Henry Lambert, S. Stürup, *Metallomics* **2015**, *7*, 885–895.

[37] C. J. Murgas, S. P. Green, A. K. Forney, R. M. Korba, S.-S. An, T. Kitten, H. R. Lucas, *ACS Infect. Dis.* **2020**, *6*, 1906–1921.

[38] J. Schur, A. Lüning, A. Klein, R. W. Köster, I. Ott, *Inorg. Chim. Acta* **2019**, *495*, 118982.

[39] P. Hikisz, Ł. Szczupak, A. Koceva-Chyła, A. Guśpiel, L. Oehninger, I. Ott, B. Therrien, J. Solecka, K. Kowalski, *Molecules* **2015**, *20*, 19699–19718.

[40] T. V. Serebryanskaya, A. S. Lyakhov, L. S. Ivashkevich, J. Schur, C. Frias, A. Prokop, I. Ott, *Dalton Trans.* **2015**, *44*, 1161–1169.

[41] F. Liu, F. Pei, A. M. Mariga, L. Gao, G. Chen, L. Zhao, *J. Food Drug Anal.* **2015**, *23*, 630–635.

[42] J. Schur, C. M. Manna, A. Deally, R. W. Köster, M. Tacke, E. Y. Tshuva, I. Ott, *Chem. Commun.* **2013**, *49*, 4785.

[43] S. I. Kirin, I. Ott, R. Gust, W. Mier, T. Weyhermüller, N. Metzler-Nolte, *Angew. Chem. Int. Ed.* **2008**, *47*, 955–959; *Angew. Chem.* **2008**, *120*, 969–973.

[44] I. Ott, H. Scheffler, R. Gust, *ChemMedChem* **2007**, *2*, 702–707.

[45] Z. Garda, E. Molnár, N. Hamon, J. L. Barriada, D. Esteban-Gómez, B. Váradi, V. Nagy, K. Pota, F. K. Kálmán, I. Tóth, N. Lihi, C. Platas-Iglesias, É. Tóth, R. Tripier, G. Tircsó, *Inorg. Chem.* **2021**, *60*, 1133–1148.

[46] D. Ndiaye, M. Sy, A. Pallier, S. Même, I. de Silva, S. Lacerda, A. M. Nonat, L. J. Charbonnière, É. Tóth, *Angew. Chem. Int. Ed.* **2020**, *59*, 11958–11963; *Angew. Chem.* **2020**, *132*, 12056–12061.

[47] S. Laine, C. S. Bonnet, F. K. Kálmán, Z. Garda, A. Pallier, F. Caillé, F. Suzenet, G. Tircsó, É. Tóth, *New J. Chem.* **2018**, *42*, 8012–8020.

[48] M. Yu, M. B. Ward, A. Franke, S. L. Ambrose, Z. L. Whaley, T. M. Bradford, J. D. Gorden, R. J. Beyers, R. C. Cattley, I. Ivanović-Burmazović, D. D. Schwartz, C. R. Goldsmith, *Inorg. Chem.* **2017**, *56*, 2812–2826.

[49] E. M. Gale, I. P. Atanasova, F. Blasi, I. Ay, P. Caravan, *J. Am. Chem. Soc.* **2015**, *137*, 15548–15557.

[50] E. M. Gale, S. Mukherjee, C. Liu, G. S. Loving, P. Caravan, *Inorg. Chem.* **2014**, *53*, 10748–10761.

[51] G. S. Loving, S. Mukherjee, P. Caravan, *J. Am. Chem. Soc.* **2013**, *135*, 4620–4623.

[52] C. Policar, J. Bouvet, H. C. Bertrand, N. Delsuc, *Curr. Opin. Chem. Biol.* **2022**, *67*, 102109.

[53] R. Bonetta, *Chem. Eur. J.* **2018**, *24*, 5032–5041.

[54] C. Policar, in *Redox-Active Therapeutics* (Eds.: I. Batinic-Haberle, J. Reboucas, I. Spasojević), Springer Science, New York, **2016**, pp. 125–164.

[55] I. Batinic-Haberle, A. Tovmasyan, I. Spasojevic, *Redox Biol.* **2015**, *5*, 43–65.

[56] S. Miriyala, I. Spasojevic, A. Tovmasyan, D. Salvemini, Z. Vujaskovic, D. St Clair, I. Batinic-Haberle, *Biochim. Biophys. Acta Mol. Basis Dis.* **2012**, *1822*, 794–814.

[57] O. Iranzo, *Bioorg. Chem.* **2011**, *39*, 73–87.

[58] I. Batinić-Haberle, J. S. Rebouças, I. Spasojević, *Antioxid. Redox Signaling* **2010**, *13*, 877–918.
[59] S. Signorella, C. Palopoli, G. Ledesma, *Coord. Chem. Rev.* **2018**, *365*, 75–102.
[60] J. D. Aguirre, V. C. Culotta, *J. Biol. Chem.* **2012**, *287*, 13541–13548.
[61] J. P. Lisher, D. P. Giedroc, *Front. Cell. Infect. Microbiol.* **2013**, *3*, https://doi.org/10.3389/fcimb.2013.00091.
[62] F. Basolo, R. G. Pearson, *Mechanisms of Inorganic Reactions a Study of Metal Complexes in Solution*, Wiley, New York, **1967**.
[63] M. Gerloch, E. C. Constable, *Transition Metal Chemistry*, VCH, New York, **1994**.
[64] H. Irving, R. J. P. Williams, *J. Chem. Soc.* **1953**, 3192–3210.
[65] H. Irving, R. J. P. Williams, *Nature* **1948**, *162*, 746–747.
[66] Y. Inada, T. Sugata, K. Ozutsumi, S. Funahashi, *Inorg. Chem.* **1998**, *37*, 1886–1891.
[67] S. F. Lincoln, A. E. Merbach in *Advances in Inorganic Chemistry* (Eds.: A. G. Sykes), Academic Press, San Diego, **1995**, pp. 1–88.
[68] P. Flis, L. Ouerdane, L. Grillet, C. Curie, S. Mari, R. Lobinski, *New Phytol.* **2016**, *211*, 1129–1141.
[69] G. Schanne, M. Zoumpoulaki, G. Gazzah, A. Vincent, H. Preud'homme, R. Lobinski, S. Demignot, P. Seksik, N. Delsuc, C. Policar, *Oxid. Met.Cell. Longev.* **2022**, *2022*, e3858122.
[70] M. J. Cohen, F. W. Karasek, *J. Chromatogr. Sci.* **1970**, *8*, 330–337.
[71] J. C. May, J. A. McLean, *Anal. Chem.* **2015**, *87*, 1422–1436.
[72] R. Cumeras, E. Figueras, C. E. Davis, J. I. Baumbach, I. Gràcia, *Analyst* **2015**, *140*, 1376–1390.
[73] G. A. Eiceman, Z. Karpas, H. H. Hill, Jr., *Ion Mobility Spectrometry*, CRC Press, Boca Raton, **2013**.
[74] E. Kalenius, M. Groessl, K. Rissanen, *Nat. Chem. Rev.* **2019**, *3*, 4–14.
[75] F. Lanucara, S. W. Holman, C. J. Gray, C. E. Eyers, *Nat. Chem.* **2014**, *6*, 281–294.
[76] B. A. Link, A. J. Sindt, L. S. Shimizu, T. D. Do, *Phys. Chem. Chem. Phys.* **2020**, *22*, 9290–9300.
[77] A. Kruve, K. Caprice, R. Lavendomme, J. M. Wollschläger, S. Schoder, H. V. Schröder, J. R. Nitschke, F. B. L. Cougnon, C. A. Schalley, *Angew. Chem. Int. Ed.* **2019**, *58*, 11324–11328; *Angew. Chem.* **2019**, *131*, 11446–11450.
[78] D. Liu, M. Chen, Y. Li, Y. Shen, J. Huang, X. Yang, Z. Jiang, X. Li, G. R. Newkome, P. Wang, *Angew. Chem. Int. Ed.* **2018**, *57*, 14116–14120; *Angew. Chem.* **2018**, *130*, 14312–14316.
[79] E. R. Brocker, S. E. Anderson, B. H. Northrop, P. J. Stang, M. T. Bowers, *J. Am. Chem. Soc.* **2010**, *132*, 13486–13494.
[80] Z. Du, R. E. F. de Paiva, K. Nelson, N. P. Farrell, *Angew. Chem. Int. Ed.* **2017**, *56*, 4464–4467; *Angew. Chem.* **2017**, *129*, 4535–4538.
[81] D. M. Templeton, F. Ariese, R. Cornelis, L.-G. Danielsson, H. Muntau, H. P. van Leeuwen, R. Lobinski, *Pure Appl. Chem.* **2000**, *72*, 1453–1470.
[82] F. Cisnetti, A.-S. Lefèvre, R. Guillot, F. Lambert, G. Blain, E. Anxolabéhère-Mallart, C. Policar, *Eur. J. Inorg. Chem.* **2007**, 4472–4480.
[83] S. Durot, C. Policar, F. Cisnetti, F. Lambert, J.-P. Renault, G. Pelosi, G. Blain, H. Korri-Youssoufi, J.-P. Mahy, *Eur. J. Inorg. Chem.* **2005**, 3513–3523.
[84] C. Policar, S. Durot, F. Lambert, M. Cesario, F. Ramiandrasoa, I. Morgenstern-Badarau, *Eur. J. Inorg. Chem.* **2001**, 1807–1818.
[85] A.-S. Bernard, C. Giroud, H. Y. V. Ching, A. Meunier, V. Ambike, C. Amatore, M. G. Collignon, F. Lemaître, C. Policar, *Dalton Trans.* **2012**, *41*, 6399–6403.
[86] W. H. Koppenol, D. M. Stanbury, P. L. Bounds, *Free Radical Biol. Med.* **2010**, *49*, 317–322.
[87] A. Vincent, M. Thauvin, E. Quévrain, E. Mathieu, S. Layani, P. Seksik, I. Batinic-Haberle, S. Vriz, C. Policar, N. Delsuc, *J. Inorg. Biochem.* **2021**, *219*, 111431.
[88] A. Vincent, J. R. Fores, E. Tauziet, E. Quévrain, Á. Dancs, A. Conte-Daban, A.-S. Bernard, P. Pelupessy, K. Coulibaly, P. Seksik, C. Hureau, K. Selmeczi, C. Policar, N. Delsuc, *Chem. Commun.* **2020**, *56*, 399–402.
[89] P. Seksik, H. Sokol, V. Grondin, C. Adrie, H. Duboc, B. Pigneur, G. Thomas, L. Beaugerie, G. Trugnan, J. Masliah, M. Bachelet, *Innate Immun.* **2010**, *16*, 381–390.
[90] C. Lenoir, C. Sapin, A. H. Broquet, A.-M. Jouniaux, S. Bardin, I. Gasnereau, G. Thomas, P. Seksik, G. Trugnan, J. Masliah, M. Bachelet, *Life Sci.* **2008**, *82*, 519–528.
[91] J. M. McCord, I. Fridovich, *J. Biol. Chem.* **1969**, *244*, 6049–6055.
[92] R. F. Pasternack, B. Halliwell, *J. Am. Chem. Soc.* **1979**, *101*, 1026–1031.
[93] R. D. Shannon, *Acta Crystallogr. Sect. A* **1976**, *32*, 751–767.
[94] J. M. Andrić, M. Z. Misini-Ignjatović, J. S. Murray, P. Politzer, S. D. Zarić, *ChemPhysChem* **2016**, *17*, 2035–2042.
[95] V. Gabelica, E. Marklund, *Curr. Opin. Chem. Biol.* **2018**, *42*, 51–59.
[96] K. Michelmann, J. A. Silveira, M. E. Ridgeway, M. A. Park, *J. Am. Soc. Mass Spectrom.* **2015**, *26*, 14–24.
[97] M. E. Ridgeway, M. Lubeck, J. Jordens, M. Mann, M. A. Park, *Int. J. Mass Spectrom.* **2018**, *425*, 22–35.
[98] J. R. N. Haler, C. Kune, P. Massonnet, C. Comby-Zerbino, J. Jordens, M. Honing, Y. Mengerink, J. Far, E. De Pauw, *Anal. Chem.* **2017**, *89*, 12076–12086.

M. Zoumpoulaki, G. Schanne, N. Delsuc, H. Preud'homme, E. Quévrain, N. Eskenazi, G. Gazzah, R. Guillot, P. Seksik, J. Vinh, R. Lobinski, C. Policar*

Deciphering the Metal Speciation in Low-Molecular-Weight Complexes by IMS-MS: Application to the Detection of Manganese Superoxide Dismutase Mimics in Cell Lysates

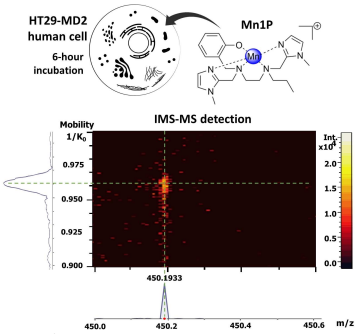

Ion mobility spectrometry (IMS) effectively distinguishes between first-row divalent transition metal complexes, despite very similar ionic radii of the ions. The speciation study of two Mn-based superoxide dismutase (SOD) mimetics (or mimics) was performed in intricate cell lysates using IMS coupled to mass spectrometry (IMS-MS). Quantification was performed by comparison with a standard consisting of an analogous $^{13}C_6$-Co^{II} heavy ligand.